

Passive alignment stability and auto-alignment of multipass amplifiers based on Fourier transforms

Karsten Schuhmann^{1,2,*}, Klaus Kirch^{1,2}, Andreas Knecht², Mirosław Marszałek², Francois Nez³, Jonas Nuber², Randolph Pohl⁴, Ivo Schulthess¹, Laura Sinkunaite², Manuel Zeyen¹, and Aldo Antognini^{1,2}

¹Institute for Particle Physics and Astrophysics, ETH, 8093 Zurich, Switzerland

²Paul Scherrer Institute, 5232 Villigen PSI, Switzerland

³Laboratoire Kastler Brossel, UPMC-Sorbonne Universités, CNRS, ENS-PSL Research University, Collège de France, 75005 Paris, France.

⁴Johannes Gutenberg-Universität Mainz, QUANTUM, Institut für Physik & Exzellenzcluster PRISMA, 55128 Mainz, Germany

*Corresponding author: skarsten@phys.ethz.ch

March 18, 2019

Abstract

This study investigates the stability to tilts (misalignments) of Fourier-based multi-pass amplifiers, i.e., amplifiers where a Fourier transform is used to transport the beam from pass to pass. Here, the stability properties of these amplifiers to misalignments (tilts) of their optical components has been investigated. For this purpose, a method to quantify the sensitivity to tilts based on the amplifier small-signal gain has been elaborated and compared with measurements. To improve on the tilt stability by more than an order of magnitude a simple auto-alignment system has been proposed and tested. This study, combined with other investigations devoted to the stability of the output beam to variations of aperture and thermal lens effects of the active medium, qualifies the Fourier-based amplifier for the high-energy and the high-power sector.

1 Introduction

Multipass laser amplifiers are used to boost the output energy of laser oscillators owing to their smaller losses and higher damage thresholds [1, 2, 3, 4]. Because of their apparent simplicity, typically less attention is devoted to the design of multipass amplifiers compared to oscillators [5, 6, 7].

Multipass amplifiers are commonly based on relay imaging (4f-imaging) from active medium to active medium as the imaging provides identical beam size for

each passes at the active medium. The propagation in the 4f-based amplifier takes thus the simple form [8]

$$AM - 4f - AM - 4f - AM - 4f \dots ,$$

where AM indicates a pass on the active medium, and 4f a relay imaging. However, in this design the changes of the phase front curvature caused by the thermal lens at the active medium are adding up from pass to pass, resulting in output beam characteristics (size, divergence, quality) strongly dependent on the thermal lens of the active medium.

In this study, Fourier-based multipass amplifiers are considered, i.e., multipass amplifiers where the propagation from active medium to active medium is accomplished using an optical Fourier transform. The beam propagation in the Fourier-based amplifiers takes the form [9]

$$AM - Fourier - AM - SP - AM - Fourier \\ - AM - SP - AM - Fourier - AM - SP - AM \dots ,$$

where SP represents a short free propagation and Fourier any propagation that performs an optical Fourier transform. In contrast to the 4f-based amplifiers, Fourier-based amplifiers show output beam characteristics which are independent on variations of the thermal lens ensued by the pumped active medium [9]. This relies on the peculiar property of the optical Fourier transform that inverts the phase front curvature, so that the phase front distortions

occurring in one pass at the active medium are canceled (in first order) by the successive pass [9]. Another advantage of the Fourier-based design is the transverse mode cleaning that occurs from the interplay between Fourier transform and soft aperture effects at the active medium, favoring TEM00-mode operation. Therefore, the Fourier-based design represents an alternative to 4f-based designs especially at the energy and power frontiers where the thermal lens becomes one of the paramount limitations.

The concept of Fourier-based amplifiers has been introduced in [10] and successively elaborated in [11, 12, 13, 14, 9], where a detailed comparison between Fourier-based and state-of-the-art multipass amplifiers based on the 4f-relay imaging is presented. In contrast to these earlier considerations, here another crucial aspect of laser design is considered, namely, the stability of the amplifier performance to misalignments (tilts).

This study reveals that Fourier-based designs have also excellent (passive) stability properties for misalignments (tilts). Furthermore, it demonstrates theoretically and practically, that the Fourier-based design is well apt for a simple auto-alignment system that mitigates the beam excursion from the optical axis (perfect alignment) caused by the tilts of its various optical components. Hence, this study, combined with the investigations of [9], displays the excellent performance of the Fourier-based architecture with respect to thermal lens variations, aperture effects, beam quality, efficiency and alignment stability, qualifying it for high-power and high-energy applications.

2 Method to evaluate the misalignment sensitivity

The following procedure is undertaken to evaluate the sensitivity of the considered multipass amplifiers to misalignments. First, the size of the fundamental Gaussian beam (TEM00 mode) propagating in the amplifier is evaluated with the ABCD-matrix formalism applied to the complex Gaussian beam parameter q . A complex ABCD-matrix is used to model the aperture effect occurring in the active medium [6, 14, 9]. As a second step, the excursion of the Gaussian beam from the optical axis (the beam propagates on the optical axis for perfect alignment) is computed making use of the ABCD-matrix formalism applied to the geometrical ray describing the axis of the Gaussian beam. For this purpose, another ABCD-matrix must be defined, describing the aperture effects to this ray propagation. The excursion of the laser beam from the optical axis can be used as a measure of the sensitivity of the multipass system to misalignment effects. Knowledge of this excursion can be exploited also to compute the decrease of the multipass amplifier gain caused by the misalignments.

The dependency of the gain (transmission) on tilts constitutes the sensitivity of the multipass amplifier to mirror tilts.

In this study, it is assumed that losses in the multipass system occur only at the active medium whose position-dependent gain (and absorption in the unpumped region) can be approximated by an average gain and a position-dependent transmission function (soft aperture) [9]. It is further assumed that the soft aperture of the active medium can be fairly approximated by a Gaussian aperture [5, 6, 9, 14], i.e., an aperture with Gaussian intensity transmission function τ :

$$\tau(x, y) = e^{-\frac{x^2+y^2}{W^2}}, \quad (1)$$

where x and y are the transverse distances from the optical axis and W the radius where the intensity is decreased to $1/e^2$. Such an aperture transforms an input Gaussian beam with $1/e^2$ -radius w_{in} , excursion x_{in} and angle θ_{in} w.r.t. the optical axis into an output Gaussian beam with $1/e^2$ -radius w_{out} , excursion x_{out} and angle θ_{out} given by

$$1/w_{out}^2 = 1/w_{in}^2 + 1/W^2, \quad (2)$$

$$x_{out} = x_{in} \frac{W^2}{w_{in}^2 + W^2}, \quad (3)$$

$$\theta_{out} = \theta_{in} - x_{in} \frac{w_{in}^2}{w_{in}^2 + W^2} \frac{1}{R}, \quad (4)$$

where R is the phase front radius of the beam at the aperture position. Note that the phase front radius R remains unaltered when the beam passes the aperture:

$$R_{out} = R_{in} \equiv R. \quad (5)$$

Figure 1 can be used to deduce these equations relating the beam parameters before and after the aperture. The relations expressed in Eqs. (2)-(5) can be captured into the ABCD-matrix formalism. Two ABCD-matrices can be defined to describe the Gaussian aperture at the active medium: the first applies to the complex parameter q defined as [5, 6]

$$\frac{1}{q} = \frac{1}{R} - i \frac{\lambda}{\pi w^2}, \quad (6)$$

where λ is the wavelength of the laser beam, w and R the local $1/e^2$ -radius and phase front radius of the beam, respectively. The corresponding ABCD-matrix is obtained from Eqs. (2) and (5). It takes the form

$$M_{aperture}^q = \begin{bmatrix} 1 & 0 \\ -i \frac{\lambda}{\pi W^2} & 1 \end{bmatrix}. \quad (7)$$

$M_{aperture}^q$ is used to compute the size (w) and phase front radius (R) evolution along the propagation using the relation [5, 6]

$$q_{out} = \frac{Aq_{in} + B}{Cq_{in} + D} = \frac{q_{in}}{-i \frac{\lambda}{\pi W^2} q_{in} + 1}, \quad (8)$$

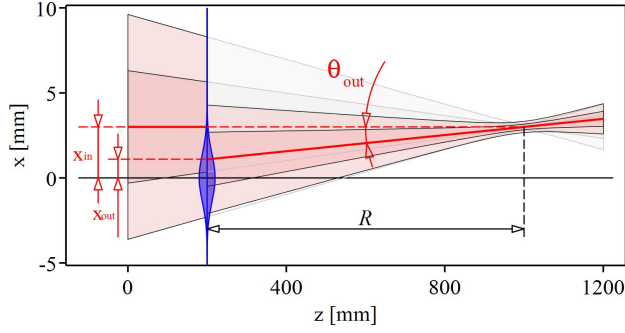


Figure 1: Scheme showing the effect of a soft aperture on the beam propagation. The aperture whose transmission function is depicted by the blue area decreases the beam excursion from x_{in} at the input plane to x_{out} at the output plane because it selects only part of the beam. Moreover, a non-vanishing excursion of the beam at the impact plane ($x_{in} \neq 0$) results in a change of the output beam angle θ_{out} . Geometrical considerations can be used to deduce that $\theta_{out} - \theta_{in} = (x_{out} - x_{in})/R$. In this scheme it is assumed that the input beam is moving parallel to the optical axis, i.e. $\theta_{in} = 0$. Yet, the aperture does not affect the position of the beam focus. The darker and lighter shaded red areas indicate the $\pm w$ and the $\pm 2w$ size of the beam.

where q_{in} and q_{out} are the q -parameters before and after the aperture, respectively.

The second ABCD-matrix applies to the geometrical propagation of the beam axis and is obtained building on Eqs. (3) and (4):

$$M_{\text{aperture}}^{\text{geometry}} = \begin{bmatrix} \frac{W^2}{w_{in}^2 + W^2} & 0 \\ -\frac{w_{in}^2}{w_{in}^2 + W^2} \frac{1}{R} & 1 \end{bmatrix}. \quad (9)$$

$M_{\text{aperture}}^{\text{geometry}}$ is used to calculate the excursion x_{out} and angle θ_{out} after passing the aperture:

$$\begin{bmatrix} x_{out} \\ \theta_{out} \end{bmatrix} = \begin{bmatrix} \frac{W^2}{w_{in}^2 + W^2} & 0 \\ -\frac{w_{in}^2}{w_{in}^2 + W^2} \frac{1}{R} & 1 \end{bmatrix} \begin{bmatrix} x_{in} \\ \theta_{in} \end{bmatrix}. \quad (10)$$

Similar equations are valid for the other transverse direction (y -direction).

As visible from Eq. (2), the passage through an aperture reduces the beam size, thereby generating power and intensity losses. For a Gaussian beam on the optical axis, the power transmission through the aperture is given by

$$T_{\text{aperture}}^{\text{aligned}} = \frac{W^2}{w_{in}^2 + W^2}. \quad (11)$$

This transmission is further decreased when the beam has

an offset from the optical axis of x_{in} and y_{in} :

$$T_{\text{aperture}}^{\text{mis-aligned}} = e^{-2 \frac{x_{in}^2 + y_{in}^2}{w_{in}^2 + W^2}} \frac{W^2}{w_{in}^2 + W^2}. \quad (12)$$

The power transmission T_{tot} through the amplifier is obtained by multiplying the transmissions of each pass at the active medium:

$$T_{\text{tot}} = \prod_{n=1}^N T_{\text{aperture}}^{\text{mis-aligned}}[n], \quad (13)$$

with N representing the total number of passes at the active medium (or media) and $T_{\text{aperture}}^{\text{mis-aligned}}[n]$ the transmission at the n -th pass which depends on the beam size w_{in} , on the deviation from the optical axis x_{in} and y_{in} , and on the size of the aperture W at the n -th pass.

It is important to note that this formalism assumes Gaussian apertures and Gaussian beams. As mentioned before a Gaussian aperture transforms a Gaussian beam into a Gaussian beam of different size. A non-Gaussian aperture, on the contrary, leads to excitation of higher-order transverse beam components. Yet, in the Fourier-based amplifier design presented here, the higher-order components produced in one pass are filtered out in the next pass by the aperture itself. Hence, the TEM00 component dominates, validating the use of Gaussian beams. In this paper $W = 4w_{in}$ is assumed because a Gaussian aperture with $W = 4w_{in}$ produces a similar reduction of the fundamental mode size and a similar reduction of the fundamental mode transmission compared to a super-Gaussian aperture fulfilling the relation $w_{in} \approx 0.7R_p$ [15, 14, 16], where R_p is the radius of the super-Gaussian pump spot. The latter relation is a rule of thumb typically applied in the thin-disk laser community as it provides most efficient laser operation in the fundamental mode. The assumption $W \approx 4w_{in}$ when $w_{in} \approx 0.7R_p$ is confirmed in Sec. 4 by the measurement of the small signal gain versus tilt angles.

3 Realization of a multi-pass amplifier based on Fourier transform propagations

The investigations of alignment stability of Fourier-based amplifiers presented in this study are based without loss of generality on the specific thin-disk multi-pass amplifier shown in Fig. 2. The working principle of thin-disk lasers [17, 18, 19, 20, 21] is not presented in this work as it is of minor relevance for the argumentation exposed. In this amplifier, the beam is reflected and amplified 8 times (8-pass amplifier) on the disk while it is propagating between mirror M2 and mirror M1b. The various passes having slightly different beam paths are realized using an ar-

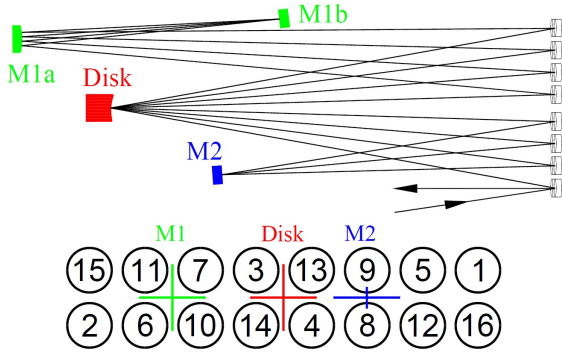


Figure 2: (Top) Scheme of the realized Fourier-based amplifier with the corresponding beam path. The beam routing in the multipass amplifier is sustained by an array of flat mirrors. (Bottom) Front view on the mirror array and its working principle. The mirrors #1 to #16 are numbered according to the sequence the beam passes them. The beam enters the amplifier over array mirror #1 and is reflected by the disk to #2, from there over M1 (M1a-M1b-M1a) to #3, over the disk to #4, over M2 to #5, and so forth until the disk is passed 8 times. The crosses indicate the position of M1, M2 and disk “projected” on the mirror array. They act as point reflectors in the mirror array plane for the propagation from mirror to mirror. Hereby we denote as mirror M1 the two-mirror system given in green composed of the convex mirror M1a and the “end-mirror” M1b.

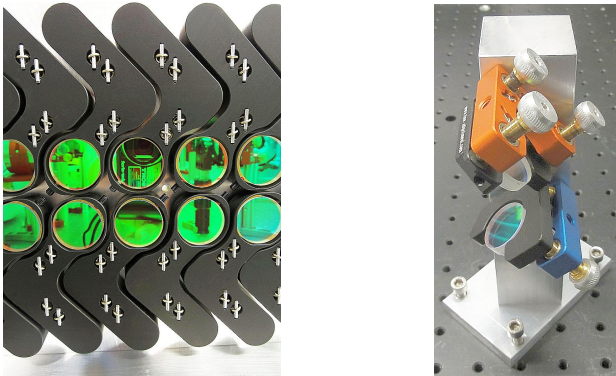


Figure 3: (Right) Photo of the custom designed mirror array with L-shaped adjustable mirror holders. The horizontal spacing between the 1” mirrors is 31 mm. (Left) Picture of the pair of 45° mirrors acting as vertical retro-reflector that can assume the functionality of the mirror M2 in Fig. 2.

ray of flat mirrors whose working principle is shown in the bottom part of Fig. 2. L-shaped mirror holders were developed and placed as shown in Fig. 3 to maximize tilt stability of the individual mirrors while minimizing the array size. Commercially available mirror holders with similar alignment stability are significantly larger leading to substantially larger spacing between the mirrors. The small size of the mirror array decreases the astigmatism related to incident angles and it guarantees that the various path lengths (especially between elements with non-vanishing dioptric power) are similar for all passes so that the beam size is reproduced from pass to pass. For the same reason, the multi-pass propagation is designed to have same M1a, M1b, M2 and disk for all passes. In the design presented in this paper the disk and M1a have a non-vanishing dioptric power while M1b, M2 and the array mirrors are flat. This choice reduces the complexity and the costs and also simplifies the alignment procedure as only the radii of curvature of the mirror M1a and the distances M1a-disk and M1a-M1b must be adapted to realize the desired layout with the same beam size at each pass.

The back and forth propagation between the disk (AM) and M1 is described by an ABCD-matrix approximatively of the form

$$M_{AM-M1-AM} \approx \begin{bmatrix} 0 & B \\ 1/B & 0 \end{bmatrix} \quad (14)$$

which corresponds to the ABCD-matrix of a Fourier transform (see Ref. [9] for more details). Differently, the back and forth propagation from the disk to M2, corresponds approximately to a short free propagation so that its ABCD-matrix takes the form

$$M_{AM-M2-AM} \approx \begin{bmatrix} 1 & L \\ 0 & 1 \end{bmatrix}, \quad (15)$$

with a length L short compared with the Rayleigh length of the beam, i.e. with $L \ll \pi w_0^2 / \lambda$, where w_0^2 is the beam waist. Note that the beam size between the AM and mirror M2 is large and that the dioptric power of the mirror M2 is either zero or a minor correction to the free propagation. Thus, the multipass amplifier depicted in Fig. 2 follows the scheme

$$\begin{aligned} & AM - Fourier - AM - SP - AM - Fourier \\ & - AM - SP - AM - Fourier - AM - SP - AM - \dots \end{aligned}$$

In this paper, the focus is on the stability properties of this Fourier-based multi-pass amplifier w.r.t. misalignments (tilts), especially of the active medium. Two amplifier configurations based on the scheme of Fig. 2 are investigated: in the first configuration the M2 mirror is a flat back-reflecting mirror (acting almost as a “end-mirror”), in the second configuration, the mirror M2 is replaced by a pair of mirrors oriented at 45° as shown in Fig. 3 (b) that acts as a vertical (y-direction) retro-reflector.

4 Sensitivity of a multipass amplifier to misalignment

The excursion of the laser beam from the optical axis while propagating in the multipass amplifier of Fig. 2 is shown in Fig. 4. It has been calculated using the ABCD-matrix

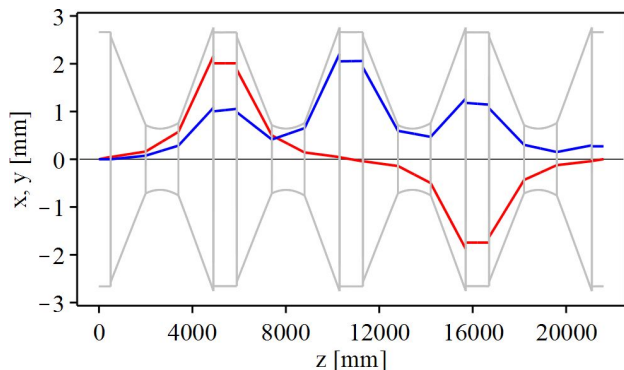


Figure 4: Excursion of the Gaussian beam axis w.r.t. the optical axis along the propagation in the Fourier-based amplifier of Fig. 2 computed using the ABCD-matrix formalism applied to ray optics and including aperture effects. The blue curve represents the beam excursion for a disk tilt of $\phi = 50 \mu\text{rad}$. The red curve represents the beam excursion for an input beam with an angle of $100 \mu\text{rad}$, w.r.t. a perfect alignment. As a comparison, the beam size evolution $\pm w$ along the propagation axis z is shown by the grey curves. An aperture width of $W = 10 \text{ mm}$ has been used in these plots. The vertical lines represent the positions of the disk (with a focusing dioptric power) and the positions of the defocusing mirror M1a, respectively. These plots apply for both the horizontal (x -) and the vertical (y -) directions.

formalism applied to the geometric ray representing the Gaussian beam axis. Aperture effects at the disk have been included via the ABCD-matrix of Eq. (10) and are visible in Fig. 4 by the sudden decrease of the beam size at the disk. The excursion of the propagating beam from the optical axis has been evaluated for two different types of misalignment and compared to the evolution of the beam size along the optical axis. In red is displayed the excursion for a tilt of the beam in-coupled into the multipass system, in blue for a tilt of the disk. When neglecting aperture effects, at the 8th pass there is a vanishing beam excursion for both types of misalignment. Indeed, the multiplication of the four Fourier transform matrices that take place between the 1st and the 8th pass corresponds to the identity matrix. Hence, disregarding the aperture effects and the short propagations of Eq. (15), the beam leaves the disk after the 8th pass at exactly the same position and with the same angle w.r.t. the optical axis as in the 1st pass.

In general, the beam cutoffs caused by the apertures at the active medium damp the beam excursions and angles relative to the optical axis. For the special case of the 8th pass (most stable pass with respect to thermal lens effects and thin-disk tilt), the beam angle is reduced compared to the 1st pass, but the beam position is slightly offset from the optical axis. This small excursion decreases with increasing aperture size W .

Throughout this paper, using the rule of thumb diffused in the thin-disk laser community and justified in [14] a Gaussian aperture with $W = 10 \text{ mm}$ is assumed for a pump diameter of 7 mm at FWHM, and a $1/e^2$ beam radius at the disk of $w = 2.5 \text{ mm}$.

Inspired by the studies reported in [3] also a modified version of the multipass amplifier shown in Fig. 2 has been investigated in which mirror M2 is replaced by a pair of 45° mirrors acting as a vertical (y -direction) retro-reflector. This mirror pair inverts the tilt and the excursion of the beam from the optical axis in the y -direction while it does not affect the tilt and the excursion in the x -direction. Hence, as already shown in [22], a vertical retro-reflector significantly increases the alignment stability in the vertical direction. Here, the evaluation of the alignment stability of [22] has been advanced to include aperture effects. As can be seen by comparing Fig. 5 to Fig. 4, this modification leads to a significant reduction of the beam excursions in particular for the 4th and the 5th pass but also to a reduction of the excursion and angle of the out-coupled beam (leaving the 8th pass).

Note that in the amplifier designs presented in this paper (and in the majority of the amplifier designs) the misalignment of the beam in the x - and the y -direction can be treated independently. We chose to implement a retro-reflector in vertical direction to reduce the misalignment effect caused by the hot air wedge at the front side of the disk [3, 23], reducing the sensitivity to variations of the pump power.

The use of a corner-cube reflector with 3 mirrors arranged at an angle of 54° and acting as retro-reflectors would provide inversion of the beam excursions and angles for both the horizontal and the vertical directions, resulting in an enhanced alignment stability in both directions.

The beam excursions simulated in Figs. 4 and 5 have been confirmed by measurements summarized in Fig. 6. These measurements show beam profiles and positions (excursions) for various tilts of the disk for three configurations: the first column at the 2nd pass of the Fourier-based multi-pass amplifier of Fig. 2, the second column at the 8th pass of the same amplifier, and the third column at the 8th pass of the same amplifier but the mirror M2 replaced by a pair of 45° mirrors acting as a vertical retro-reflector. Note that when a beam is reflected at a tilted disk, it acquires an angle θ w.r.t. the optical axis corre-

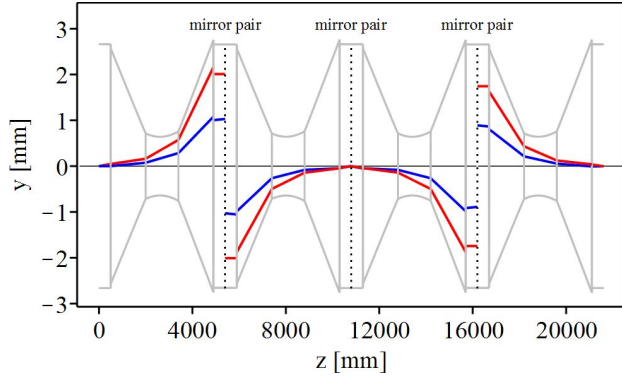


Figure 5: Similar to Fig. 4, but for a multipass amplifier where M2 is replaced by a pair of 45° mirrors acting as a vertical retro-reflector. The vertical dotted lines indicate the position of the retro-reflector. The excursion is shown only for the vertical component. The horizontal component is not affected by the vertical retro-reflector so that it follows the evolution shown in Fig. 4.

sponding to twice the disk tilt, i.e. $\theta = 2\phi$, where ϕ is the tilt of the disk axis from perfect alignment.

As predicted by the simulations of Figs. 4 and 5 the beam excursions from the unperturbed position (for $0 \mu\text{rad}$ tilts) are larger at the 2nd pass than at the 8th pass. With increasing tilt, the profile at the 8th pass (second column) is distorted. These distortions visible for a tilt of $\phi = 84 \mu\text{rad}$ originate mainly at the 4th pass, where the beam excursions are maximal (see Fig. 4). Indeed, for large excursions the aperture at the disk is poorly approximated by a Gaussian transmission function resulting in a transmitted beam with non-Gaussian (non-symmetric) profile. Larger distortions and even fringe effects occurs for a tilt of $\phi = 126 \mu\text{rad}$ at the 8th pass (second column). These fringes originate from hard apertures and beam cut-offs at the edge of optical components mostly at, or around the 4th pass, where beam excursions are maximal.

A comparison between second and third column discloses the improvements in term of stability to misalignment yielded by the use of the M2 retro-reflector. It suppresses beam excursions at the 8th pass. Even more, beam distortions originating around the 4th pass are suppressed as the retro-reflector strongly restrains the beam excursions at the intermediate passes (compare Fig. 4 to Fig. 5).

As explained in Sec. 2 an alternative way to quantify the sensitivity to misalignment effects is to measure the gain decrease of the multipass amplifier as a function of the disk tilt ϕ . The total gain through the amplifier can be readily quantified using Eqs. (11) to (13) and assuming that there are no other losses than already included in the aperture transmission of the disk. The total gain in this

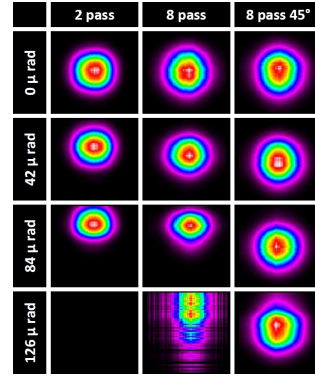


Figure 6: Measured beam profiles for various disk tilts for three multipass configurations based on Fig. 2. The colors represent the beam intensity. Each picture is normalized to its intensity maximum. These images show how beam excursions and distortions increase with misalignment. Note that the first row represents the reference point as it shows the beam position for the aligned amplifier. The first column is the excursion at the 2nd pass, the second column at the 8th pass, and the third column also at the 8th pass but for an amplifier where M2 is replaced by a pair of 45° mirrors acting as a vertical retro-reflector. The $\phi = 126 \mu\text{rad}$ tilt causes such a large beam excursion already at the second pass that the beam is deviated outside the aperture of the beam profiler used to record the images. At the 8th-pass the beam excursion as shown in Fig. 4 is much smaller so the beam enters the profiler. Yet, this beam is fully distorted because of hard aperture effects occurring at the 4th pass where the excursion is maximal. When the retro-reflector is introduced, the excursion at the 4th pass vanishes so that the beam distortions at the 8th pass disappear. This results in a beam at the 8th pass with almost a Gaussian profile and a small excursion from the unperturbed position given in the first row.

case takes the form

$$G_{8\text{-pass}}^{\text{M2-single}} \approx (G_0)^8 \left(\frac{W^2}{w_{\text{in}}^2 + W^2} \right)^8 e^{-1.07 \cdot 10^8 \phi^2} \quad (16)$$

for the 8-pass amplifier with simple M2 mirror, and

$$G_{8\text{-pass}}^{\text{M2-45}^\circ\text{-pair}} \approx (G_0)^8 \left(\frac{W^2}{w_{\text{in}}^2 + W^2} \right)^8 e^{-2.98 \cdot 10^7 \phi^2} \quad (17)$$

for the amplifier where M2 is replaced by a retro-reflector. In these equations G_0 is the gain per pass (averaged over the transverse beam profile) while the approximate symbol accounts for the small variations of the beam sizes w_{in} at the various passes and the assumption that the gain does not decrease with the number of passes (no saturation). The exponential terms in these equations encompass the losses caused by the beam excursion from the optical axis.

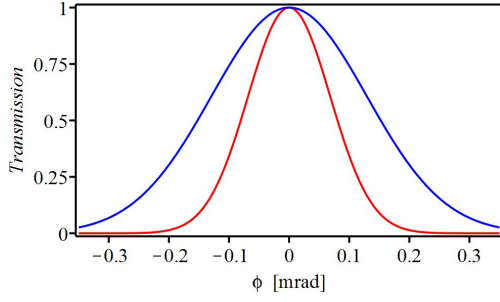


Figure 7: The red curve represents the tilt-dependent part of $G_{8\text{-pass}}^{\text{M2-single}}$ ($e^{-1.07 \cdot 10^7 \phi^2}$) for the 8-pass amplifier of Fig. 2 as a function of the disk tilt ϕ . It corresponds to the tilt-dependent transmission through the multipass amplifier normalized to 1 for vanishing tilts. Similarly, the blue curve is the tilt dependent part of $G_{8\text{-pass}}^{\text{M2-45}^\circ\text{-pair}}$ ($e^{-2.98 \cdot 10^7 \phi^2}$) for the same amplifier but M2 replaced by a retro-reflector.

A plot of the two functions $G_{8\text{-pass}}^{\text{M2-single}}$ and $G_{8\text{-pass}}^{\text{M2-45}^\circ\text{-pair}}$ is shown in Fig. 7 in red and blue, respectively.

A measurement of the total gain versus disk tilt for the two multipass amplifier configurations (M2 simple, M2 as retro-reflector) is shown in Fig. 8. The measured data were already presented in [22] but here they are compared with the theoretical predictions of Eqs. (16) and (17). It turned out that the best empirical fit functions to the measured data are given by parabola and not by Gaussian functions as predicted in Eqs. (16) and (17).

In our measurement the multipass amplifiers were not perfectly aligned so that the maximal gains were observed for non-vanishing disk tilts ($\phi = -23.3 \mu\text{rad}$ and $\phi = -15.3 \mu\text{rad}$ extrapolated using the parabolic fits). To compare the measurements to the model, the value of $(G_0)^8 \left(\frac{W^2}{w_{\text{in}}^2 + W^2}\right)^8$ of Eqs. (16) and (17) has been fixed to the gain maximum obtained from the parabolic fit. Also the angle ϕ in Eqs. (16) and (17) has been redefined to account for the offset of the maximum (see parameterizations given in Fig. 8). The resulting functions, shown by the dashed curves in Fig. 8 that assume $W = 4w_{\text{in}}$, are not fit to the data, but simply normalized to the maximum obtained from the parabolic fits. For small excursions, there is an excellent agreement between the models expressed by Eqs. (16) and (17) on the one hand and the measurements of Fig. 8 on the other hand. This agreement quantitatively confirm our assumption that the effective losses at the active medium can be described by a Gaussian aperture with $W \approx 4w_{\text{in}}$ when $w_{\text{in}} \approx 0.7R_p$.

For large tilts the measured losses exceed the theoretical predictions. Indeed, the Gaussian approximation of the aperture becomes increasingly inadequate as the beam axis approaches the edge of the super-Gaussian aperture.

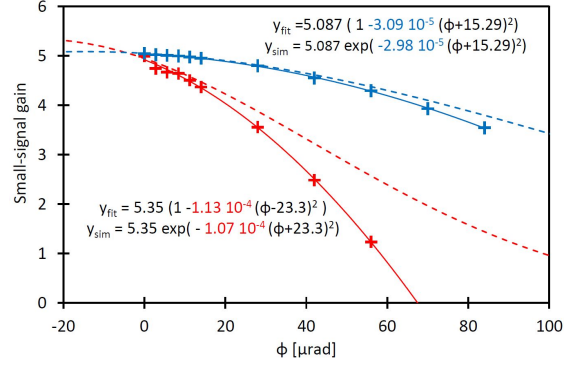


Figure 8: Small signal gain versus disk tilt in vertical direction. The red points were measured for the multi-pass amplifier of Fig. 2 with simple M2-mirror. The blue points have been obtained from the same amplifier but M2 replaced by a vertical retro-reflector. The measurements have been fitted with parabolic functions (solid lines). The dashed curves represent the predictions from Eqs. (16) and (17) normalized to match the maxima of the parabolic fits.

However, only small misalignments – which are well described by our model – are relevant for the evaluation of a laser system. Lasers with exceeding fluctuations and drifts of the output power are in fact typically unsuitable for the practical applications.

5 Reduction of alignment sensitivity using an active compensation

A significantly higher stability to misalignment can be realized by implementing a system actively controlling the alignment (tilt) of mirrors. Auto-alignment units comprising quadrant detectors (or other devices that measure the beam position) feedback loops, and motorized mirror holders are commercially available and simple to implement [24]. However, obtaining the best possible alignment using the smallest number of controls requires the correct placement of quadrant detectors and active mirrors.

In this section, a simple active stabilization system for the Fourier-based multipass amplifier of Fig. 2 is presented that compensates for tilts of the in-coupled beam, disk, M1 and M2 to overall minimize beam excursions. The attention has been focused primarily to correct for tilts of the disk, as it is prone to misalignments owing to the pumping and cooling processes that it undergoes and because of the air wedge at its surface [23]. It is assumed that the disk itself cannot be equipped with actuators to control its tilt.

Figure 9 shows the multipass amplifier of Fig. 2 upgraded with an optimal and simple active stabilization system. The input beam direction is actively controlled by the feedback loop (C1) acting on the actuators of mir-

ror M_{in} with two independent degrees of freedom (vertical and horizontal). The beam travels successively to the disk where it undergoes the first amplification and reflection. For the disk tilted (misaligned) by an angle ϕ , the beam acquires an additional angle w.r.t. the optical axis of $\Delta\theta = 2\phi$. The Fourier propagation that takes place in the propagation disk-M1b-disk transforms the tilt of the beam leaving the disk into a beam excursion when the beam returns for the second time (second pass) to the disk. At the disk, the beam suffers an additional tilt $\Delta\theta$. Because of the short propagation length between disk and M2, the excursion of the beam at the mirror M2 is dominated by the tilt of the beam after the first reflection at the disk that is given by the tilt of the disk and the tilt of the beam before impinging for the first time on the disk. The excursion of the beam at M2 can be measured by placing a quadrant detector (Q1) in the vicinity of M2 that measures the beam spuriously transmitted through M2. Any deviation of the beam position from the set point (when the amplifier is aligned) generates two error signals: one for the horizontal, the other for the vertical direction. Through the feedback loop C1, these error signals act on the actuators of mirror M_{in} to cancel the beam excursion at M2.

After reflection on mirror M2, the beam reaches the disk for the third time where it again acquires an angle $\theta = 2\phi$. This tilt once again results in an excursion from the set point position when the beam reaches M2 for the second time. The excursion of the second pass on M2 can be measured with a second quadrant detector (Q2). The error signals generated by Q2 are used to regulate the actuators of the mirror M2 through a second feedback loop C2 so that the beam excursion at the second pass on mirror M2 is nullified. The same correction (tilt) of mirror M2 automatically correct all the successive passes on M2 due to the repetitive structure of the amplifier (see Fig. 10). Both loops are sufficiently independent so that their interplay can compensate for tilts of the in-coupled beam and for tilts of the disk. The regulation can also partially compensate for tilts of M1.

Only two feedback loops are therefore sufficient to stabilize the most critical optical elements of the multipass amplifier for all passes as M1, M2, and active medium are common for all passes. Oppositely, it has to be stressed that individual mirror misalignments within the mirror array cannot be compensated by this feedback system so that high stability is required for the individual holders of the array mirrors.

Both quadrants have to be placed in the vicinity of mirror M2. It is possible to detect the position of the first pass on M2 with Q1 and of the second pass on M2 with Q2 because the two passes impinge on M2 at different angles. Thus, a short free propagation from M2 to the quadrants Q1 and Q2 can be used to separate the two spuriously transmitted beams (see Fig. 9).

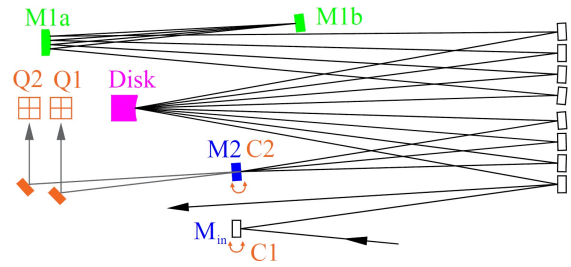


Figure 9: Schematic of the realized multipass amplifier equipped with a simple auto-alignment system. Only two loops (each with a vertical and a horizontal degree of freedom) are sufficient to mitigate the excursion of the laser beam from the optical axis for tilts of the disk, M1a, M1b, M2 and input beam. Each loop (C1 and C2) comprises a quadrant detector (Q1 and Q2) whose error signals act on the motorized mirrors M_{in} and M2, respectively. Ideally, the quadrants measure the position of the beam at the first and second pass on the M2 mirror.

In Fig. 10, the excursion of the laser beam axis from the optical axis is illustrated along the 8-pass amplifier of Fig. 9 equipped with the above-described active stabilization. Only the propagations for a tilted disk is displayed. The propagation for a tilted in-coupled beam is not shown, as a tilt of the input beam can be exactly canceled by the loop C1 so that the beam would propagate on the optical axis ($x = y = 0$) of the amplifier. The resulting excursion evolution shown in Fig. 10 can be compared with the excursions in Figs. 4 and 5. Similar overall excursions are visible but in Fig. 10 the disk tilt has been increased by a factor of 25 compared to the non-active stabilized amplifiers. Hence, the active stabilization improves greatly the stability to disk tilts.

The auto-alignment system of Fig. 9 has been tested experimentally. The measured gain decrease of the actively controlled amplifier for variations of the disk tilt is summarized in Fig. 11 and compared with the results from the non-actively stabilized amplifiers with the same optical layout. The actively stabilized amplifier shows a major (order of magnitude) decrease of the sensitivity to disk tilts. However, the measured stability improvement was smaller than predicted from simulations. This reduced performance can be ascribed to the non-vanishing M2-Q1 and M2-Q2 distances that in the realized amplifier were about 1.5 m. This issue could be solved by implementing an imaging of M2 on the two quadrants.

It is interesting to note that the number of actively controlled mirrors can be reduced to one without loss of alignment stability by eliminating the loop C2 and replacing the active mirror M2 with a corner-cube reflector with 3 mirrors arranged at an angle of 54° and acting as retro-reflectors.

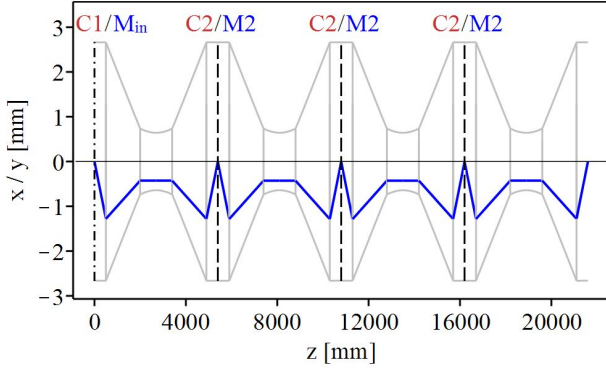


Figure 10: Similar to Fig. 4 but for a multipass amplifier equipped with the simple auto-alignment system depicted in Fig. 9. Because of the efficient compensation produced by the active stabilization, the disk tilt has been increased to $\phi = 1.25$ mrad, (a factor 25 times larger than in Fig. 4). The correction generated by C1 (steering of M_{in}) is compensating the downstream tilts occurring in the first and second pass on the disk, so that the beam excursion of the first pass on M2 is nullified. Similarly, the second loop C2 adjusts the tilt of the mirror M2 so that the beam excursions at all successive passes (third, fourth etc.) on M2 are nullified.

6 Summary

A simple model has been presented to calculate the losses occurring at the soft aperture naturally present in a pumped active medium and the effects of this aperture for the beam propagation. This knowledge has been used to quantify the misalignment sensitivity of multipass amplifiers in two ways. The first, by simply tracking the evolution of the beam excursion w.r.t. the optical axis while the beam propagates in the amplifier for a tilted (misaligned) optical element or input beam. The second, which requires the knowledge of the first, by computing the decrease of the amplifier gain as a function of the tilt of the considered optical element.

These two methods have been used to investigate the sensitivity of Fourier-based amplifiers to beam tilts. The choice of the Fourier-based amplifiers is motivated by the superior stability of these multipass amplifiers to variations of thermal lens and aperture effects at the active medium compared with state-of-the-art amplifiers based on the 4f-imaging propagation. An extensive comparison between the two multipass architectures can be found in [9]. Three variations of the same Fourier-based amplifier were investigated in this study: the basic layout of Fig. 2, the basic layout but mirror M2 replaced with a vertical retro-reflector, and the basic layout equipped with an auto-alignment system shown Fig. 9.

The simulations were compared with measurements of

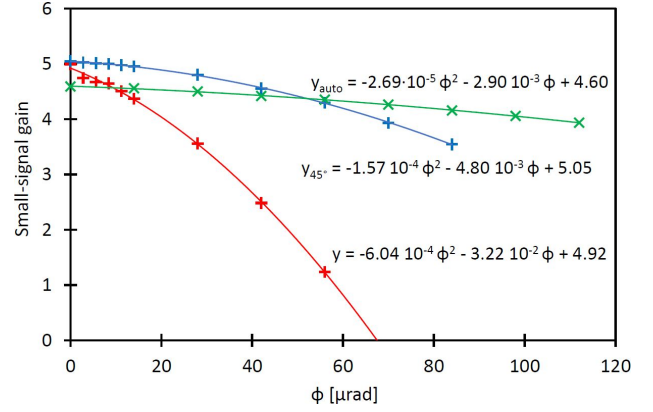


Figure 11: Measured small-signal gain for three 8-pass amplifiers versus the disk tilt ϕ . The red points have been taken for the simple amplifier of Fig. 2, the blue points for the same amplifier but M2 replaced by a vertical retro-reflector, the green ones for the amplifier of Fig. 9 equipped with the active stabilization system. Polynomial fits have been drawn to guide the eye. For the amplifier with the active stabilization system the mirror M2 has been replaced with a mirror with slightly higher transmission to generate a robust error signal from Q1 and Q2. This reduces the overall gain of the amplifier but does not alter its tilt dependence.

the amplifier gain and good agreement has been found. The stability of Fourier-based multipass amplifiers has been demonstrated via months long operation of a thin-disk laser based on the layout of Fig. 2 without the need of realignment. Furthermore, simulations and observations showed that this stability can be improved by a factor of 4 in one direction (vertical) when M2 is implemented as a pair of 45° mirrors acting as vertical retro-reflectors, or in both directions (vertical and horizontal) when M2 is implemented as a three-mirror system acting as retro-reflectors in both directions. Alike, more than an order of magnitude improvement in tilt stability can be obtained by equipping the multipass amplifier with a simple auto-alignment system comprising only two quadrant detectors and two motorized mirror holders.

These findings combined with the investigation presented in [9] fully qualifies the Fourier-based design to be the appropriate choice in the high energy and high power sector.

7 Funding information

We acknowledge the support from the Swiss National Science Foundation Project SNF 200021_165854, the European Research Council ERC CoG. #725039 and ERC StG. #279765. The study has been also supported by the

ETH Femtosecond and Attosecond Science and Technology (ETH-FAST) initiative as part of the NCCR MUST program.

References

- [1] V. Chvykov, H. Cao, R. Nagymihaly, M. P. Kalashnikov, N. Khodakovskiy, R. Glasscock, L. Ehrentraut, M. Schnuerer, and K. Osvay. High peak and average power Ti:sapphire thin disk amplifier with extraction during pumping. *Opt. Lett.*, 41(13):3017 – 3020, Jul 2016.
- [2] S. Keppler, C. Wandt, M. Hornung, R. Bödefeld, A. Kessler, A. Sävert, M. Hellwing, F. Schorcht, J. Hein, and M. C. Kaluza. Multipass amplifiers of POLARIS. *Proc. SPIE*, 8780:87800I–87800I–6, 2013.
- [3] J.-P. Negel, A. Loescher, A. Voss, D. Bauer, D. Sutter, A. Killi, M. Abdou Ahmed, and T. Graf. Ultrafast thin-disk multipass laser amplifier delivering 1.4 kW (4.7 mJ, 1030 nm) average power converted to 820 W at 515 nm and 234 W at 343 nm. *Opt. Express*, 23(16):21064 – 21077, Aug 2015.
- [4] Shigeki Tokita, Junji Kawanaka, Yasukazu Izawa, Masayuki Fujita, and Toshiyuki Kawashima. 23.7 W picosecond cryogenic Yb:YAG multipass amplifier. *Opt. Express*, 15(7):3955 – 3961, Apr 2007.
- [5] Herwig Kogelnik. On the propagation of gaussian beams of light through lenslike media including those with a loss or gain variation. *Appl. Opt.*, 4(12):1562 – 1569, Dec 1965.
- [6] A.E. Siegman. *Lasers*. University Science Books, 1986.
- [7] V. Magni. Resonators for solid-state lasers with large-volume fundamental mode and high alignment stability. *Appl. Opt.*, 25(1):107 – 117, Jan 1986.
- [8] W. W. Simmons, D. R. Speck, and J. T. Hunt. Argus laser system: performance summary. *Appl. Opt.*, 17(7):999–1005, Apr 1978.
- [9] Karsten Schuhmann, Klaus Kirch, Mirosław Marszałek, Francois Nez, Randolph Pohl, Ivo Schulthess, Laura Sinkunaite, Gunther Wichmann, Manuel Zeyen, and Aldo Antognini. Multipass amplifiers with self-compensation of the thermal lens. *Applied optics*, 57(35):10323–10333, 2018.
- [10] A. Antognini, K. Schuhmann, F. D. Amaro, F. Biraben, A. Dax, A. Giesen, T. Graf, T. W. Hansch, P. Indelicato, L. Julien, C. Y. Kao, P. E. Knowles, F. Kottmann, E. Le Bigot, Y. W. Liu, L. Ludhova, N. Moschuring, F. Mulhauser, T. Nebel, F. Nez, P. Rabinowitz, C. Schwob, D. Taquu, and R. Pohl. Thin-disk Yb:YAG oscillator-amplifier laser, ASE, and effective Yb:YAG lifetime. *IEEE Journal of Quantum Electronics*, 45(8):993 – 1005, Aug 2009.
- [11] K. Schuhmann, M.A. Ahmed, A. Antognini, T. Graf, T.W. Hansch, K. Kirch, F. Kottmann, R. Pohl, D. Taquu, A. Voss, and B. Weichelt. Thin-disk laser multi-pass amplifier. *Proceedings of SPIE, Solid state lasers XXIV: technology and devices*, 9342:93420U–, 2015.
- [12] Karsten Schuhmann, Klaus Kirch, Francois Nez, Randolph Pohl, and Aldo Antognini. Thin-disk laser scaling limit due to thermal lens induced misalignment instability. *Appl. Opt.*, 55(32):9022 – 9032, Nov 2016.
- [13] K. Schuhmann, K. Kirch, and A. Antognini. Multipass resonator design for energy scaling of mode-locked thin-disk lasers. *Proc. SPIE*, 10082:100820J–100820J–9, 2017.
- [14] Karsten Schuhmann. *The Thin-Disk Laser for the 2S 2P Measurement in Muonic Helium*. PhD thesis, Institute for Particle Physics and Astrophysics, ETH Zürich, 2017.
- [15] Yuan Han Peng, James Cheng, Yan Ying Cheah, Kin Seng Lai, Ernest Lau, and Seok Khim Ang. High brightness continuous wave ceramic Yb:LuAG thin-disk laser. *Opt. Express*, 23(15):19618–19623, Jul 2015.
- [16] Jan-Philipp Negel, Andreas Voss, Marwan Abdou Ahmed, Dominik Bauer, Dirk Sutter, Alexander Killi, and Thomas Graf. 1.1 kW average output power from a thin-disk multipass amplifier for ultrashort laser pulses. *Opt. Lett.*, 38(24):5442–5445, Dec 2013.
- [17] U. Brauch, A. Giesen, M. Karszewski, Chr. Stewen, and A. Voss. Multiwatt diode-pumped Yb:YAG thin disk laser continuously tunable between 1018 and 1053 nm. *Opt. Lett.*, 20(7):713 – 715, Apr 1995.
- [18] A. Giesen, H. Hügel, A. Voss, K. Wittig, U. Brauch, and H. Opower. Scalable concept for diode-pumped high-power solid-state lasers. *Applied Physics B*, 58(5):365 – 372, May 1994.
- [19] A. Giesen. Thin disk lasers power scalability and beam quality. *Laser Technik Journal*, 2(2):42 – 45, 2005.

- [20] A. Giesen. High-power thin-disk lasers. *Advanced Solid-State Photonics*, page MA1, 2007.
- [21] A. Giesen and J. Speiser. Fifteen years of work on thin-disk lasers: Results and scaling laws. *IEEE Journal of Selected Topics in Quantum Electronics*, 13(3):598–609, May 2007.
- [22] Karsten Schuhmann, Theodor W. Hänsch, Klaus Kirch, Andreas Knecht, Franz Kottmann, Francois Nez, Randolph Pohl, David Taqqu, and Aldo Antognini. Thin-disk laser pump schemes for large number of passes and moderate pump source quality. *Appl. Opt.*, 54(32):9400 – 9408, Nov 2015.
- [23] Tom Dietrich, Stefan Piehler, Christoph Röcker, Martin Rumpel, Marwan Abdou Ahmed, and Thomas Graf. Passive compensation of the misalignment instability caused by air convection in thin-disk lasers. *Optics letters*, 42(17):3263–3266, 2017.
- [24] Thomas Müller-Wirts. Aligna automated laser beam alignment and stabilization system, 2018. <http://www.tem-messtechnik.de/EN/aligna.htm>.